Radiation dose forecast of WASAVIES during ground-level enhancement

Ryuho Kataoka[1], Tatsuhiko Sato[2], Yûki Kubo[3], Daikou Shiota[4], Takao Kuwabara[5], Seiji Yashiro[6], and Hiroshi Yasuda[7]

[1]National Institute of Polar Research, Tachikawa, Japan, [2]Japan Atomic Energy Agency, Ibaraki, Japan, [3]National Institute of Information and Communications Technology, Koganei, Japan, [4]Solar-Terrestrial Environment Laboratory, Nagoya University, Nagoya, Japan, [5]Bartol Research Institute, Department of Physics and Astronomy, University of Delaware, Newark, Delaware, USA, [6]Department of Physics, Catholic University of America, Washington, District of Columbia, USA, [7]National Institute of Radiological Sciences, Chiba, Japan

Abstract Solar energetic particles (SEPs) sometimes induce powerful air showers that significantly increase the radiation dose at flight altitudes. In order to provide information of such a space radiation hazard to aircrew, a forecast model is developed for WASAVIES (Warning System of Aviation Exposure to SEP), based on the focused transport equation of solar protons and Monte Carlo particle transport simulation of the air shower. WASAVIES gives a simple and fast way to predict the time profile of dose rate during ground-level enhancements.

1. Introduction

Solar flares and coronal mass ejections (CMEs) generate solar energetic particles (SEPs) in the heliosphere. A fraction of SEP is sometimes energetic enough to deeply penetrate into the terrestrial atmosphere, and the high flux and high energy sometimes cause a ground-level enhancement (GLE) as measured by ground-based neutron monitors as well as a significant radiation dose of aircrews at the top of the troposphere. Such an energetic space weather event is rare, and only a total of 71 GLE have been recorded since 1943 when the first GLE was observed [*Forbush*, 1946]. The total dose of aircrews is dominated by galactic cosmic rays, but the dose rate can be higher for several hours during a GLE. As a short-term space weather forecast, it is therefore important to predict the time variation of the dose rate at flight altitude as soon as possible when GLEs occur; then the prediction can be used to understand the current situation against the whole GLE sequence to reasonably mitigate possible radiation damages.

There are a number of attempts to predict SEP profiles and to estimate the radiation dose of aircrews during GLEs. *Kubo and Akioka* [2004] utilized the soft X-rays to make an SEP alert. *Aran et al.* [2005, 2006] developed solar particle engineering code, a physics-based model to predict the time profiles of low-energy SEP accelerated by interplanetary shocks. *Nunez* [2011] developed a prediction system (http://spaceweather.uma.es/forecastpanel.htm) which analyzes soft X-rays and proton flux data to empirically forecast the >10 MeV protons. Recently, Y. Kubo (manuscript in preparation, 2014) presented a novel physics-based method to predict the recovery time profiles of SEP using the rising phase. *Mertens et al.* [2010, 2013] developed NAIRAS (Nowcast of Atmospheric Ionizing Radiation System) which provides real-time data-driven climatology of aviation environment (http://sol.spacenvironment.net/~nairas/). Other models have also been developed for postexposure evaluations [*Copeland et al.*, 2008; *Matthia et al.*, 2009].

However, there has been no physics-based forward models to predict the time profile of GLEs. In this paper we propose a forecast model, WASAVIES (Warning System for Aviation Exposure to Solar Energetic Particles), to predict the time profile of radiation dose for aircrews. After the real-time detection of GLEs by a GLE alarm system [*Kuwabara et al.*, 2006], and using the background solar wind structures [*Shiota et al.*, 2014], WASAVIES will provide predicted time profiles of radiation dose at any altitude, longitude, and latitude within 2.5 h from flare onset by the simplest manner. In this paper we report the current workflow what we do manually if another GLE happens. Automated website will be developed soon as a next step.

2. Forecast Model

Spatially one-dimensional focused transport equation can be described as

$$\frac{\partial f}{\partial t} + \mu v \frac{\partial f}{\partial z} + \mathbf{V} \cdot \nabla f + \frac{\partial p}{\partial t}\frac{\partial f}{\partial p} + \frac{\partial \mu}{\partial t}\frac{\partial f}{\partial \mu} - \frac{\partial}{\partial \mu}\left(D_{\mu\mu}\frac{\partial f}{\partial \mu}\right) = 0, \tag{1}$$
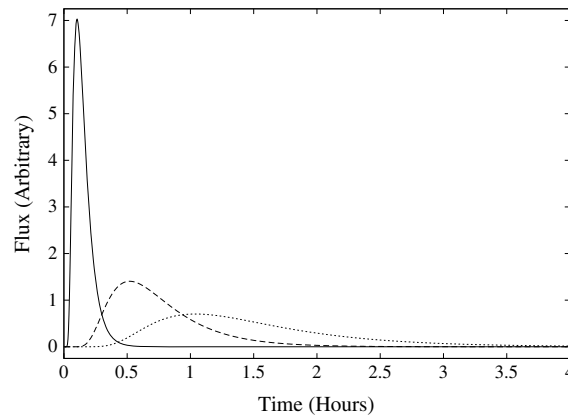
Figure 1. Injection profiles IP1 (solid), IP2 (dashed), and IP3 (dotted) as inverse Gaussian distributions. The most impulsive injection profile (IP1) is selected from the most impulsive event of GLE69 with the mean of 0.15 h and standard deviation of 0.075 h for the inverse Gaussian, and 5 times and 10 times longer time scales with fixed ratio of two for the mean and standard deviation are selected for IP2 and IP3, respectively.

where z, p, v, and μ are particle position measured along a magnetic field line, momentum intensity, speed, and pitch angle cosine, respectively. The gyrotropic phase space density f is a function of z, p, μ, and time t. **V** and $D_{\mu\mu}$ denote the solar wind velocity and pitch angle scattering coefficient, respectively. In the left-hand side of equation (1), the second to sixth terms describe particle streaming, convection by the solar wind, adiabatic deceleration, pitch angle change due to adiabatic focusing and diverging solar wind, and pitch angle scattering, respectively. It is assumed that the parallel mean free path $\lambda_\parallel$ can be written as [*Jokipii*, 1966; *Beeck and Wibberenz*, 1986]

$$\lambda_\parallel = \frac{3v}{8} \int_{-1}^{+1} \frac{(1-\mu^2)^2}{D_{\mu\mu}} \, d\mu, \qquad (2)$$

and the radial mean free path λ_r can be defined as

$$\lambda_r = \lambda_\parallel \cos^2\varphi, \qquad (3)$$

where φ is the angle between the local magnetic field direction and the radial direction. The radial mean free path is assumed to be constant across the entire interplanetary space [*Bieber et al.*, 1994]. There are several works to reproduce observations very well using this assumption [e.g., *Dröge*, 2000; *Qin et al.*, 2006].

The focused transport equation (1) was solved to obtain the time variation of the normalized proton flux at the Earth position for 18 pitch angle directions with 15 energy channels ranging from 80 MeV to 9.1 GeV. The simulated results of proton flux using several different parameter sets of mean free path and injection profile are then saved to be promptly used for air shower simulation. The injection profile at the inner boundary is expressed as an inverse Gaussian distribution (Y. Kubo, manuscript in preparation, 2014) as shown in Figure 1. The inverse Gaussian distribution is related to a diffusion process. If energetic particles are injected impulsively at a specific position in the lower corona and move outward at a constant drift rate accompanied by diffusion, the escaped particles at a specific distance in the upper corona are inverse Gaussian distributed in time. Therefore, we adopt the inverse Gaussian distribution as the particle injection time profile.

We fixed the initial power law slope of −6 in the differential rigidity spectrum, which is a typical value of GLEs [*Shea and Smart*, 2012; *Oh et al.*, 2012]. The inner boundary is at 0.05 AU, and the outer boundary is at 80 AU. The location of the inner boundary is somewhat far from the realistic releasing point of 3 solar radii [*Gopalswamy et al.*, 2012], but it does not essentially affect the obtained results in this simulation. We also fix the solar wind speed of 400 km/s and 800 km/s to determine the Parker spiral for typical and fast background events, respectively. The difference in the solar wind speed does not cause essential difference in the time profile and only affect the pitch angle distribution of the differential flux.

Observation data of GOES SEM P6 channel (80–165 MeV proton flux) is available for a total of 16 GLE events in solar cycle 23. In this paper we assumed the differential flux of the P6 channel as the approximate differential flux at 80 MeV for simplicity. As shown in Figure 1, three types of injection profiles (IP1, IP2, and IP3) are simulated to categorize the time profiles of the GLEs and to find the best fitted injection profile. Figure 2 shows example that GLE63 is best fitted
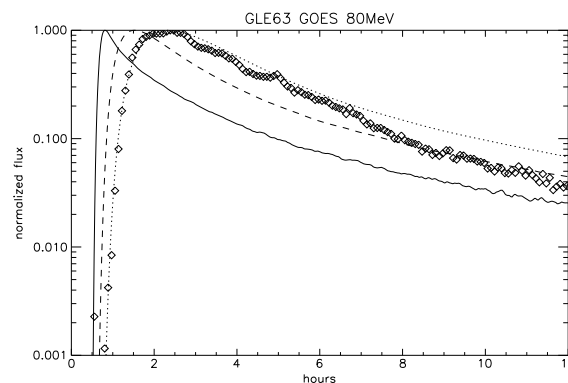

Figure 2. An example of simulated 80 MeV proton flux for the mean free path of 0.4 AU at 1.0 GeV protons with injection profiles of IP1 (solid), IP2 (dashed), and IP3 (dotted). Normalized observed profile (diamonds) is given from GLE63, which is best fitted by IP3.
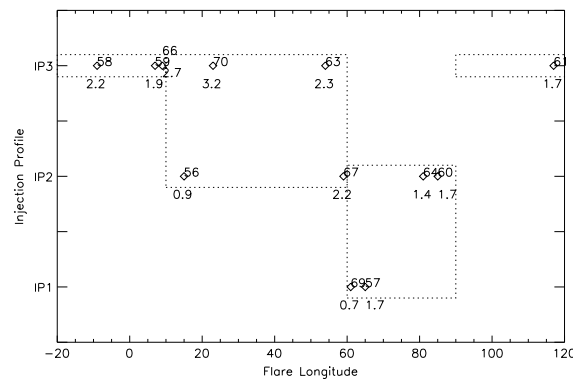
Figure 3. Scatterplot for the injection profiles against the heliolongitude of flares. Dotted areas show the possible selection of injection profiles for a given heliolongitude. GLE numbers and the time interval (in hours) between the flare onset and GOES 80 MeV flux peak are shown above and below, respectively.

by IP3. Simulated proton flux at 80 MeV is pitch angle averaged and is compared with the observed time profile to find best fitted parameters of injection profile and mean free path. It is found that the mean free path of 0.4 AU can be used as a typical value for all of the GLEs in solar cycle 23. Here we use the Parker spiral with the solar wind speed of 400 km/s rather than 800 km/s as the typical background [see *Masson et al.*, 2012, Table 1] to evaluate the correlation coefficient for all of the events. We simply use the flare onset time [*Gopalswamy et al.*, 2012, Table 1] minus 8.3 min as the zero time for our simulations. It is also found that the injection profile depends on the longitude of flare site (Figure 3), and we have a good reason to select the most impulsive one for well-connected

position, and less impulsive one for others. Further, we can select the most probable injection profile even when the flare longitude is close to 60° and we have all three possible injection profiles, by comparing with real-time neutron monitor data of GLE-alarm system [*Kuwabara et al.*, 2006] about the rising phase of GLEs. The importance of the careful choice of injection profile and the quantitative difference for the different profiles are described in section 4.

Gyromotion of negatively charged protons at energy ranging from 80 MeV to 10 GeV is calculated in an empirical magnetic field [*Tsyganenko*, 1989] to estimate the asymptotic direction [*Smart et al.*, 2000]. The T89 model gives a realistic enough magnetosphere at certain universal time and is simply parameterized by the Kp index, i.e., 3 h geomagnetic activity index, which is the best appropriate for our purpose of prediction without detailed information of interplanetary magnetic field in the near future. From the top of atmosphere of 80 km altitude at a target position of geographical coordinate system (latitude and longitude), a negatively charged proton is vertically launched, and the gyromotion by the Lorentz force is simply calculated using a standard fourth-order Runge-Kutta method until the particle exits the 10 R_E distance from the center of the Earth. The exit point is recorded to estimate the asymptotic direction, and the simulated differential flux at the asymptotic direction is sampled as the differential flux of the top of the atmosphere at the target position, assuming the same flux in the space and the top of atmosphere. If the negatively charged proton is trapped in the magnetosphere, we insert zero flux. The corresponding differential proton fluxes are then assumed as isotropic at the top of atmosphere. They are converted to the aircrew doses at any flight condition using the response function [*Sato et al.*, 2013a], which was developed on the basis of air shower simulation performed by a Monte Carlo Particle and Heavy Ion Transport code System [*Sato et al.*, 2013b].
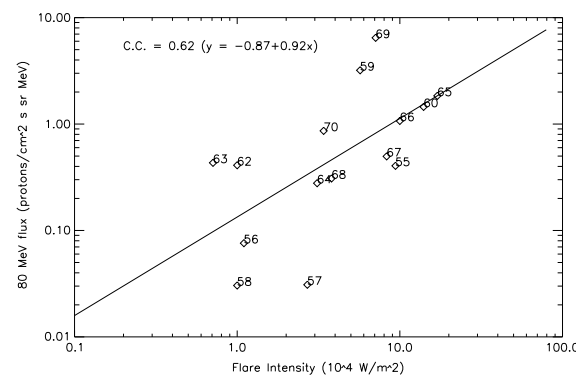

Figure 4. Approximate linear relationship between GOES X-ray (0.1–0.8 nm) flare amplitude and peak flux of GOES P6 (80–165 MeV) proton flux of the event.

3. Workflow of WASAVIES

The physics-based forward model as shown in section 2 works just after the detection of GLE onset by the GLE alarm system [*Kuwabara et al.*, 2006]. We use the reconstructed solar wind structures [*Shiota et al.*, 2014] in real time by Space-weather-forecast-Usable System Anchored by Numerical Operations and Observations (SUSANOO) project (http://st4a.stelab.nagoya-u.ac.jp/susanoo/) to select the slow- or fast-type Parker spiral for the pitch angle sampling, and we use the current Kp index to make the T89 magnetic field. The mean free path of 1 GeV proton is fixed at 0.4 AU, and Figure 3 gives the possible injection profiles by dotted areas for a
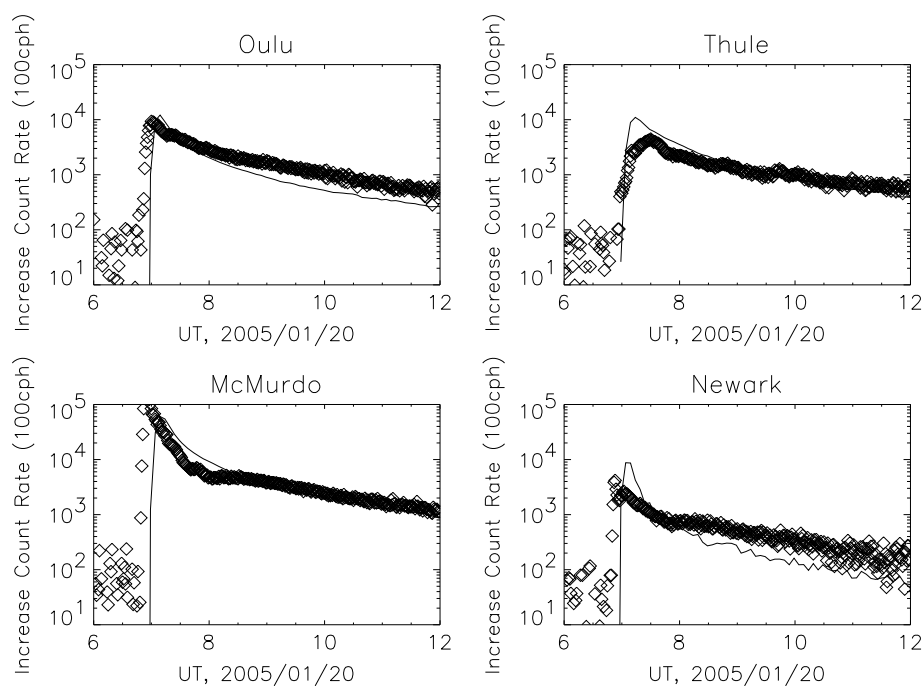
Figure 5. Simulated (solid curve) and observed (diamonds) increase count rate of neutron monitors at Oulu, Thule, McMurdo, and Newark during the GLE69 (61° heliolongitude).

given heliolongitude. However, the physics-based model shown in section 2 gives only the normalized time profile, and the amplitude must be given independently. The fastest and simplest way to calibrate the amplitude is to use the empirical relationship between the peak value of 80 MeV protons flare size (Figure 4). This gives the amplitude correction and provisional prediction of time profiles in half an hour. Slower but more accurate way is to directly use the observed peak value of real-time 80 MeV proton flux of GOES
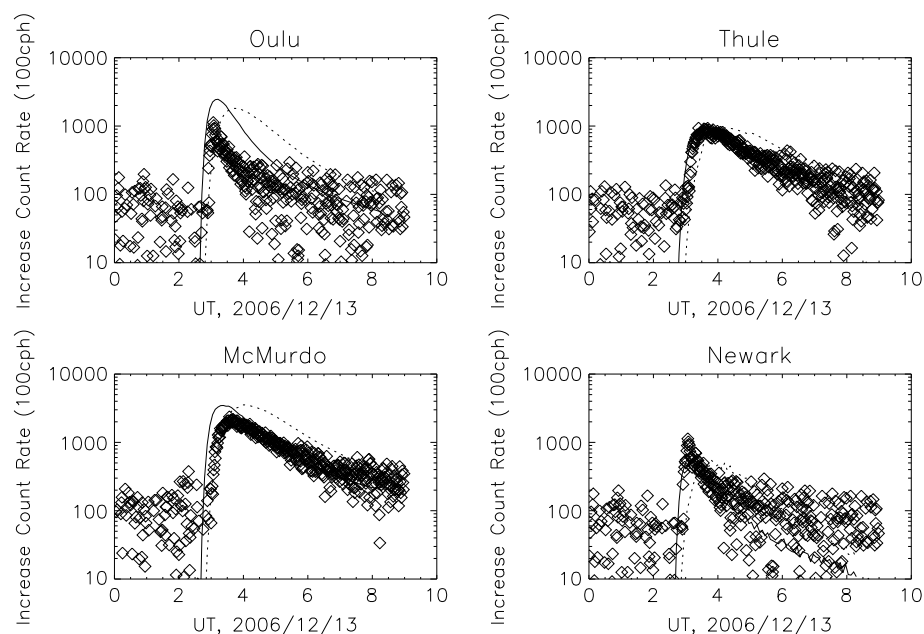

Figure 6. Simulated (solid curve: IP2, dotted curve: IP3) and observed (diamonds) increase count rate of neutron monitors at Oulu, Thule, McMurdo, and Newark during the GLE70 (23° heliolongitude).
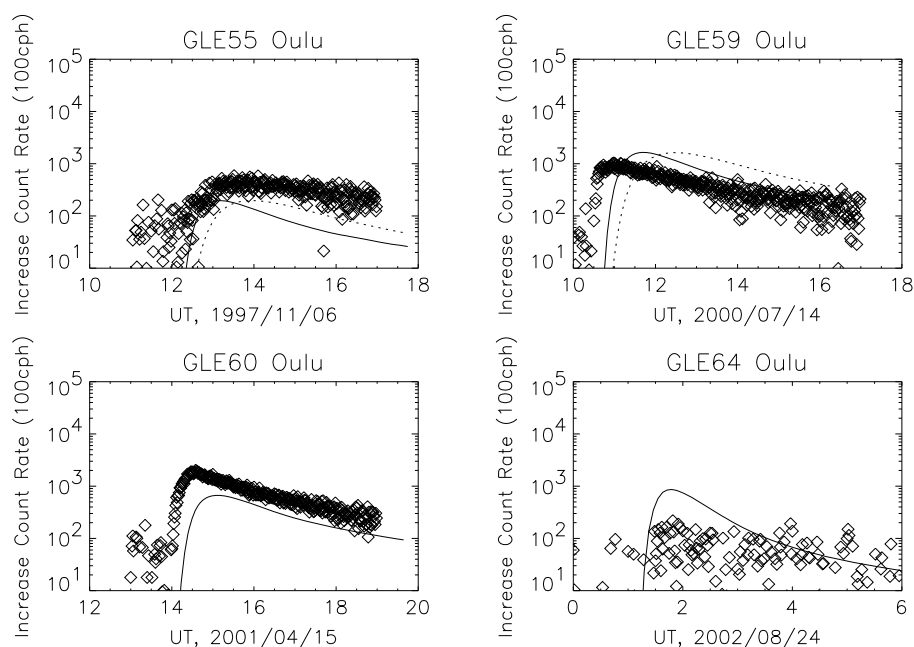
Figure 7. Other minor GLE events as observed (diamonds) at Oulu station during GLE 55 (63°), GLE 59 (7°), GLE 60 (85°), and GLE 64 (81° heliolongitude). Solid and dotted curves show the simulated profiles by WASAVIES using IP2 and IP3, respectively.

SEM P6 channel. It depends on the event, but the peak flux is typically observed within 2.5 h after the flare onset during solar cycle 23 as shown in the numbers (in hours) below triangles in Figure 3.

4. Evaluation and Limitation

In order to evaluate the errors and limitations of WASAVIES, especially to judge the asymmetry of dose rate over the world, we made some comparisons of our prediction time profiles with the observed data at several neutron monitors of which the high-resolution data are available for this study. For the strongest event of GLE69, it is shown that WASAVIES gives reasonable prediction of the time profile with the error of a factor of 2 (Figure 5). A post event analysis for GLE70 is shown in Figure 6. It is found that the parameter IP2 (solid curve) shows a better agreement for ground-based neutron monitor data, although IP3 (dotted curve) was the best fitted injection profile using the GOES P6 data. This example shows the importance of using real-time neutron monitor data to mitigate the prediction error of WASAVIES.

The simulated results by WASAVIES are also checked for all of the other minor GLEs as observed by Oulu station (GLE 55, 59, 60, and 64) during the solar cycle 23 (Figure 7). The onset and peak timing has an error of an order of 30 min, and the amplitude error is within a factor of 2. It is also found that the slowly declining profile of GLE55 can be fitted by only significantly changing the injection profile from that of the other events. GLE 62 and GLE 65 show the same problem, and these three events are not shown in Figure 3. Such a slow component may be due to the contribution of protons accelerated by interplanetary shocks.

5. Discussion

As shown in the section 4, WASAVIES roughly reproduces the observations with the typical parameter selections of the initial power law of −6, mean free path of 0.4 AU at 1.0 GeV protons, and Parker spiral of 400 km/s, by only changing the injection profiles. It is very interesting to note that such a simple setting creates the wide varieties of GLEs by the inherent geomagnetic field structures.

WASAVIES gives the simplest start point, and a lot of improvements are awaited. In this study, we assumed the same proton flux at geosynchronous orbit and at the top of atmosphere at 80 MeV, based on theoretical balance between mirroring and focusing fluxes in an ideal dipole magnetic field. The "penetration factor," i.e., the actual ratio between the proton flux at geosynchronous orbit and at top of atmosphere, deviated from
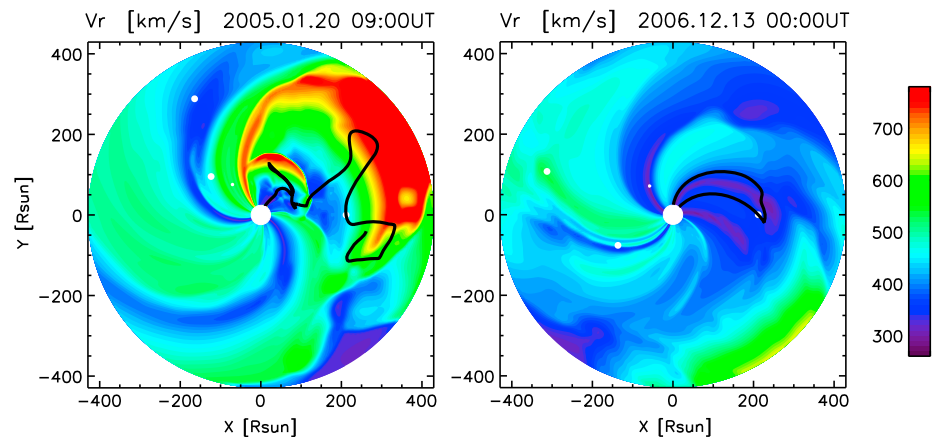
Figure 8. Realistic reconstruction of the solar wind speed distribution in the inner heliosphere by SUSANOO project during (left) GLE69 and (right) before GLE70. The Earth is located at the position ($X = 215$, $Y = 0$). A series of CMEs propagate westward for GLE69. Black lines show the magnetic field lines traced back from the Earth's position.

the unity may cause an error of roughly 50% [*Bornebusch et al.*, 2010] in the energy range of an order of 100 MeV. It would therefore be important to evaluate the penetration factor more carefully to reduce the potential errors.

It has been known that the speed of CMEs is essentially important to improve the physics-based model of SEP and GLEs [*Gopalswamy et al.*, 2012]. Next challenge would therefore be to use the CME speed to self-consistently simulate the peak amplitude as well as the injection profiles of the proton flux [*Kataoka et al.*, 2011]. How to understand, model, and predict the time variation of the proton energy spectrum itself is a very interesting and important scientific topic of future research and contributes to understand the fundamental generation mechanisms of GeV protons in the inner heliosphere. Real-time detection of CME speed within a few hours after flare onset would be very important for the forecast of GLE time profiles, and a possible correlation between the propagation speed of EUV waves and CME speed may also be useful for the forecast purpose because the EUV wave speed can be detected within half an hour after the flare onset.

Distribution of interplanetary magnetic field in the inner heliosphere is also essentially important to improve the physics-based model. WASAVIES uses Parker spiral to keep the simplicity and consistency, but the actual connectivity of magnetic field lines to the Earth, the path length, and mean free path would only be correctly understood by a very realistic three dimensional MHD simulation. For example, a simulation of the background solar wind configuration of the inner heliosphere is provided in real time by the SUSANOO project [*Shiota et al.*, 2014], and they are preparing to include realistic CMEs in their model as shown in Figure 8 as a next step. Such a global modeling of the realistic solar wind structures in the inner heliosphere including CMEs would therefore be very important to advance this field of research.

References

Aran, A., B. Sanahuja, and D. Lario (2005), Fluxes and fluences of SEP events derived from SOLPENCO, *Ann. Geophys.*, *23*, 3047–3053, doi:10.5194/angeo-23-3047-2005.

Aran, A., B. Sanahuja, and D. Lario (2006), SOLPENCO: A solar particle engineering code, *Adv. Space Res.*, *37*, 1240–1246.

Beeck, J., and G. Wibberenz (1986), Pitch angle distributions of solar energetic particles and the local scattering properties of the interplanetary medium, *Astrophys. J.*, *311*, 437–450.

Bieber, J. W., W. H. Matthaeus, C. W. Smith, W. Wanner, M.-B. Kallenrode, and G. Wibberentz (1994), Proton and electron mean free paths: The Palmer consensus revisited, *Astrophys. J.*, *420*, 294.

Bornebusch, J. P., J. M. Wissing, and M.-B. Kallenrode (2010), Solar particle precipitation into the polar atmosphere and their dependence on hemisphere and local time, *Adv. Space Res.*, *45*, 632–637.

Copeland, K., H. H. Sauer, F. E. Duke, and W. Friedberg (2008), Cosmic radiation exposure of aircraft occupants on simulated high-latitude flights during solar proton events from 1 January 1986 through 1 January 2008, *Adv. Space Res.*, *42*, 1008–1029.

Dröge, W. (2000), The rigidity dependence of solar particle scattering mean free paths, *Astrophys. J.*, *537*, 1073–1079.

Forbush, S. E. (1946), Three unusual cosmic-ray increases possibly due to charged particles from the Sun, *Phys. Rev.*, *70*(9–10), 771–772.

Gopalswamy, N., H. Xie, S. Yashiro, S. Akiyama, P. Makela, and I. G. Usoskin (2012), Properties of ground level enhancement events and the associated solar eruptions during solar cycle 23, *Space Sci. Rev.*, *171*, 23–60, doi:10.1007/s11214-012-9890-4.

Jokipii, J. R. (1966), Cosmic-ray propagation. I. Charged particles in a random magnetic field, *Astrophys. J.*, *146*, 480.

Kataoka, R., T. Sato, and H. Yasuda (2011), Predicting radiation dose on aircraft from solar energetic particles, *Space Weather*, *9*, S08004, doi:10.1029/2011SW000699.

Kubo, Y., and M. Akioka (2004), Existence of thresholds in proton flares and application to solar energetic particle alerts, *Space Weather, 2*, S01002, doi:10.1029/2004JF000164.

Kuwabara, T., J. W. Bieber, J. Clem, P. Evenson, and R. Pyle (2006), Development of a ground level enhancement alarm system based upon neutron monitors, *Space Weather, 4*, S10001, doi:10.1029/2006SW000223.

Masson, S., P. Demoulin, S. Dasso, and K.-L. Klein (2012), The interplanetary magnetic structure that guides solar relativistic particles, *Astron. Astrophys., 538*, A32, doi:10.1051/0004-6361/201118145.

Matthia, D., B. Heber, G. Reitz, M. Meier, L. Sihver, T. Berger, and K. Herbst (2009), Temporal and spatial evolution of the solar energetic particle event on 20 January 2005 and resulting radiation doses in aviation, *J. Geophys. Res., 114*, A08104, doi:10.1029/2009JA014125.

Mertens, C. J., B. T. Kress, M. Wiltberger, S. R. Blattnig, T. S. Slaba, S. C. Solomon, and M. Engle (2010), Geomagnetic influence on aircraft radiation exposure during a solar energetic particle event in October 2003, *Space Weather, 8*, S03006, doi:10.1029/2009SW000487.

Mertens, C. J., M. M. Meier, S. Brown, R. B. Norman, and X. Xu (2013), NAIRAS aircraft radiation model development, dose climatology, and initial validation, *Space Weather, 11*, 603–635, doi:10.1002/swe.20100.

Nunez, M. (2011), Predicting solar energetic proton events (E > 10 MeV), *Space Weather, 9*, S07003, doi:10.1029/2010SW000640.

Oh, S. Y., J. W. Bieber, J. Clem, P. Evenson, R. Pyle, Y. Yi, and Y.-K. Kim (2012), South Pole neutron monitor forecasting of solar proton radiation intensity, *Space Weather, 10*, S05004, doi:10.1029/2012SW000795.

Qin, G., M. Zhang, and J. R. Dwyer (2006), Effect of adiabatic cooling on the fitted parallel mean free path of solar energetic particles, *J. Geophys. Res., 111*, A08101, doi:10.1029/2005JA011512.

Sato, T., R. Kataoka, H. Yasuda, Y. Seiji, T. Kuwabara, D. Shiota, and Y. Kubo (2013a), Air shower simulation for WASAVIES: Warning system for aviation exposure to solar energetic particles, *Radiat. Prot. Dosim.*, doi:10.1093/rpd/nct332.

Sato, T., et al. (2013b), Particle and Heavy Ion Transport Code System PHITS, version 2.52, *J. Nucl. Sci. Technol., 50*, 913–923.

Shea, M. A., and D. F. Smart (2012), Space weather and the ground-level solar proton events of the 23rd solar cycle, *Space Sci. Rev., 171*, 161–188.

Shiota, D., R. Kataoka, Y. Miyoshi, T. Hara, C. Tao, K. Masunaga, Y. Futaana, and N. Terada (2014), Inner heliosphere MHD modeling system applicable to space weather forecasting for the other planets, *Space Weather, 12*, doi:10.1002/2013SW000989.

Smart, D. F., M. A. Shea, and E. O. Fluckiger (2000), Magnetospheric models and trajectory computations, *Space Sci. Rev., 93*, 305–333.

Tsyganenko, N. A. (1989), A magnetospheric magnetic field model with a warped tail current sheet, *Planet. Space Sci., 37*, 5–20.